RSC Advances

PAPER

View Article Online
View Journal | View Issue

Cite this: *RSC Adv.*, 2023, **13**, 11547

Efficient Cr(VI) removal by expanded graphite synergized with oxalic acid under UV irradiation†

Ling Zhang, Yanqing Sun, * Jie Sun and Fengming Cao

Expanded graphite (EG), an easily-obtained carbon material with the potential of transferring electrons, was utilized successfully in the removal of hazardous hexavalent chromium (Cr(VI)) by environment-friendly oxalic acid (Ox) under UV irradiation. EG with a unique worm-like structure was obtained *via* a facile microwave treatment. The results showed that the EG + Ox + UV system had optimum performance, removing 99.32% of the Cr(VI) (1 mM) within 60 min at pH = 3, and the kinetic rate constant of Cr(VI) elimination was 7.95 mol L^{-1} min^{-1}. Three components are potentially involved in the Cr(VI) elimination mechanism by the EG + Ox + UV system: (1) the direct electron transfer (DET) pathway of the EG-Ox-Cr(VI) through the acceleration effect of EG caused the majority removal of Cr(VI) under UV; (2) $\cdot CO_2^-$ generated from Ox photolysis was used to reduce some Cr(VI); (3) $\cdot CO_2^-$ created from Cr(VI)–Ox complexes in the solution through the photoinduced electron transfer (PET) pathway also reduced a little Cr(VI). Overall, the efficient removal of Cr(VI) by the EG + Ox + UV system provided new ideas for future research on Cr(VI) treatment.

Received 22nd February 2023
Accepted 29th March 2023

DOI: 10.1039/d3ra01207g

rsc.li/rsc-advances

1. Introduction

Most recently, chromium-containing wastewater has become one of the most threatening water pollutants worldwide.[1] The main existences of chromium in chromium-containing wastewater are both hexavalent (Cr(VI)) and trivalent (Cr(III)) chromium. Cr(III) is barely harmful or even non-toxic, while Cr(VI) is famous for its serious carcinogenesis or gene mutation damage to the human body due to its high toxicity.[2] In order to control chromium pollution, it is particularly crucial to eliminate Cr(VI) from water.

The process of adsorption can effectively remove Cr(VI) from water considering the benefits of simple operation, low price, and less secondary pollution,[3,4] but subsequent desorption processes are complicated, and Cr(VI) still has a high level of toxicity because adsorption simply transfers Cr(VI) from the solution to the adsorbate. The method of reduction can effectively remove hazardous Cr(VI) from water by converting Cr(VI) to Cr(III). Especially, the chemical reduction method is widely used in the industry, in which traditional inorganic reductants (such as SO_2, $NaHSO_3$, and $FeSO_4$) are commonly used.[5] Although this method is easy and efficient to operate, it is still limited to the requirement of an excess amount of the reductant and the needed treatment of the large amounts of the by-produced sludge.

Oxalic acid (Ox), the most widely distributed and highest-content small-molecule organic acid in nature, is effective at removing Cr(VI) from the environment.[6] As an organic reductant, Ox can be oxidized and released as CO_2 after participating in the reaction, which is identified as a promising green reductant with good environmental friendliness. However, because it often takes months to years for Ox to directly reduce Cr(VI),[7] it is vital to improving the reduction effect of Ox. The introduction of ultraviolet (UV),[8] Fe(III),[9,10] and catalysts[11,12] can speed up the efficiency at which Ox reduces Cr(VI) to some extent, but the effect is still not satisfactory enough due to various problems.

In recent years, the development of carbon materials has received widespread attention. Due to abundant conjugated structures, carbon materials are confirmed to act as conductors to transfer electrons between two redox components.[13] Xu *et al.*[14] used a lactic acid/biochar system to achieve the reductive elimination of Cr(VI). Although lactic acid is a weak electron donor, biochar can not only effectively enhance the direct electron transfer of lactic acid to Cr(VI) through conjugated structures and surface functional groups, but also act as a certain electron donor, resulting in the efficient Cr(VI) elimination. Kong *et al.*[15] successfully activated peracetic acid to remove micropollutants using the similar electron shuttle effect of reduced graphene oxide. Therefore, it is feasible to use carbon materials to mediate the reduction of Cr(VI) by Ox. Expanded graphite (EG), an easily-obtained functional carbon material, has received attention in water pollution treatment due to its unique loose and porous structure, low density, and good stability.[16,17] The study of EG mainly focuses on

School of Environmental and Chemical Engineering, Shanghai University, 99 Shangda Road, Shanghai 200444, PR China. E-mail: wqbiss@163.com

† Electronic supplementary information (ESI) available. See DOI: https://doi.org/10.1039/d3ra01207g

adsorption, though the Cr(VI) adsorption capacity of EG is only about 0.28 mg g^{-1}.[18] Similar to other graphitic materials, EG has abundant interlayer electrons,[19] which makes it a potential electron donor for Cr(VI) reduction. Besides, under the effect of conjugated structures, EG is likely to act as a shuttle to enhance the electron transfer from Ox to Cr(VI) under UV,[20] forming an effective synergistic Cr(VI) removal effect. Differently, because of the special physical structure, EG can float on water and receive more light,[21] which may be more favorable for Cr(VI) photoreduction However, reports on the Cr(VI) photochemical reduction by EG synergized with Ox have not yet appeared.

In this study, EG was chosen to cooperate with Ox in the photoreduction of Cr(VI) in an aqueous solution with UV exposure. On the elimination of Cr(VI) by the EG + Ox + UV system, the impacts of the initial concentration of Ox and Cr(VI), EG dosage, co-existing ions, and the reusability of EG were explored. The reduction product of Cr(VI) was also validated by UV-vis spectroscopy. By studying the impact of the solution's starting pH, observing the trend variation (pH and Ox concentration) of the solution during the reaction, and performing radical scavenging experiments, the mechanism of Cr(VI) elimination by the EG + Ox + UV system was also discussed. Investigations using scanning electron microscopy (SEM), X-ray diffractometry (XRD), Fourier transform infrared (FT-IR) spectroscopy, X-ray photoelectron spectroscopy (XPS), Mott–Schottky, and electrochemical impedance spectroscopy (EIS) curves further confirmed the unique role of EG in Cr(VI) elimination *via* the EG + Ox + UV system.

2. Materials and methods

2.1. Chemicals and materials

Expandable graphite (50 mesh) was obtained from Qingdao Kingzhilai Graphite Co., Ltd. Potassium dichromate ($K_2Cr_2O_7$), sodium hydroxide (NaOH), hydrochloric acid (HCl), oxalic acid ($H_2C_2O_4$), diphenyl carbazide ($C_{13}H_{14}N_4O$), sulfuric acid (H_2SO_4), phosphoric acid (H_3PO_4), acetone (C_3H_6O), potassium nitrate (KNO_3), sodium chloride (NaCl), sodium carbonate (Na_2CO_3), sodium phosphate monobasic (NaH_2PO_4), isopropanol (IPA), carbon tetrachloride (CCl_4), titanium trichloride ($TiCl_3$) (Sinopharm Chemical Reagent Co., Ltd.) and naphthoquinone (BQ) (Shanghai Linen Technology Development Co., Ltd.) were analytical purity.

2.2. Preparation of EG

EG was obtained from expandable graphite by microwave treatment: 5 g of 50 mesh expandable graphite was placed within the ceramic bowl and placed into the microwave oven (WP800TL23-K5, Galanz). After heating for 30 s at a working power of 800 W, the worm-like fluffy particles were obtained and sealed for use.

2.3. Characterizations

The specific morphologies of materials were examined by a Hitachi SU-1510 SEM. XRD (Rigaku/max-2550V, Hitachi) with Cu Kα radiation (40 kV, 40 MA) was used to characterize the crystal structure of materials. FT-IR spectra were recorded in a region from 500–4000 cm^{-1} by an FT-IR spectrometer (Nicolet-380, Thermo Fisher) to determine the functional groups in materials. XPS (K-Alpha, Thermo Fisher) was obtained under a monochromatic Al Kα X-ray source (1486.60 eV). A UV-Vis spectrophotometer (8453, Agilent) and a visible spectrophotometer (722, Tairen) were used to monitor the reaction process. A pH meter (PHS-25, Yueping) was used to determine the solution's pH. An electrochemical workstation was used to measure the Mott–Schottky and EIS curves of materials (CHI660E, CH Instruments).

2.4. Experiments of Cr(VI) removal

In a typical experiment, Cr(VI) (1.0 mM) and Ox (5.0 mM) were added to a 40 ml solution containing 20 mg of EG to disperse, and the pH of the solution was adjusted to 3 using 1 M NaOH or HCl. The mixture was placed into a photochemical reactor for the reaction after being magnetically stirred in the dark for 30 min (a 250 W high-pressure mercury lamp was applied as the UV light source). Following the extraction of 1 ml of the reaction solution at various time intervals for measurements, the Cr(VI) concentration was measured using diphenylcarbazide spectrophotometry at 540 nm. The efficiency of Cr(VI) removal was determined as eqn (1).

$$E\% = 100\% \times (C_0 - C_t)/C_0 \quad (1)$$

where C_0 represents the Cr(VI) concentration at the start of the reaction and C_t represents the Cr(VI) concentration at reaction time t.

In different univariate experiments, the initial Ox concentration levels were set to 0.5, 1.0, 3.0, and 5.0 mM, the initial EG dosage level were 0.25, 0.5, 0.75, and 1 g L^{-1} with the initial Cr(VI) concentration level set to 0.5, 1.0, 1.5, and 2.0 mM. Cl^-, CO_3^{2-}, NO_3^-, and $H_2PO_4^-$ at a concentration of 1 mM were chosen as co-existing ions. All the experiments were examined at room temperature.

The Ox concentration during the reaction was measured by a $TiCl_3$ color development method.[22]

To further understand the process of Cr(VI) elimination within the EG + Ox + UV system, the pseudo-zero-order, pseudo-first-order, and pseudo-second-order kinetic models were used to model the experimental results.

To verify the reusability of EG in the system, the used EG was obtained by filtration, washing thoroughly with 1 M HCl, and drying for recycling experiments and characterization.

3. Results and discussion

3.1. Removal of Cr(VI) by the EG + Ox + UV system

Fig. 1(a) shows the elimination of Cr(VI) in various systems. Cr(VI) concentration was little changed after 60 min with Ox, showing that it was difficult to reduce Cr(VI). 2.56% of Cr(VI) was removed when EG was used, indicating the slow and weak adsorption of EG for Cr(VI). When EG and Ox were used together, 46.68% of Cr(VI) was removed. This showed that the EG + Ox system enhanced the removal of Cr(VI) to a certain

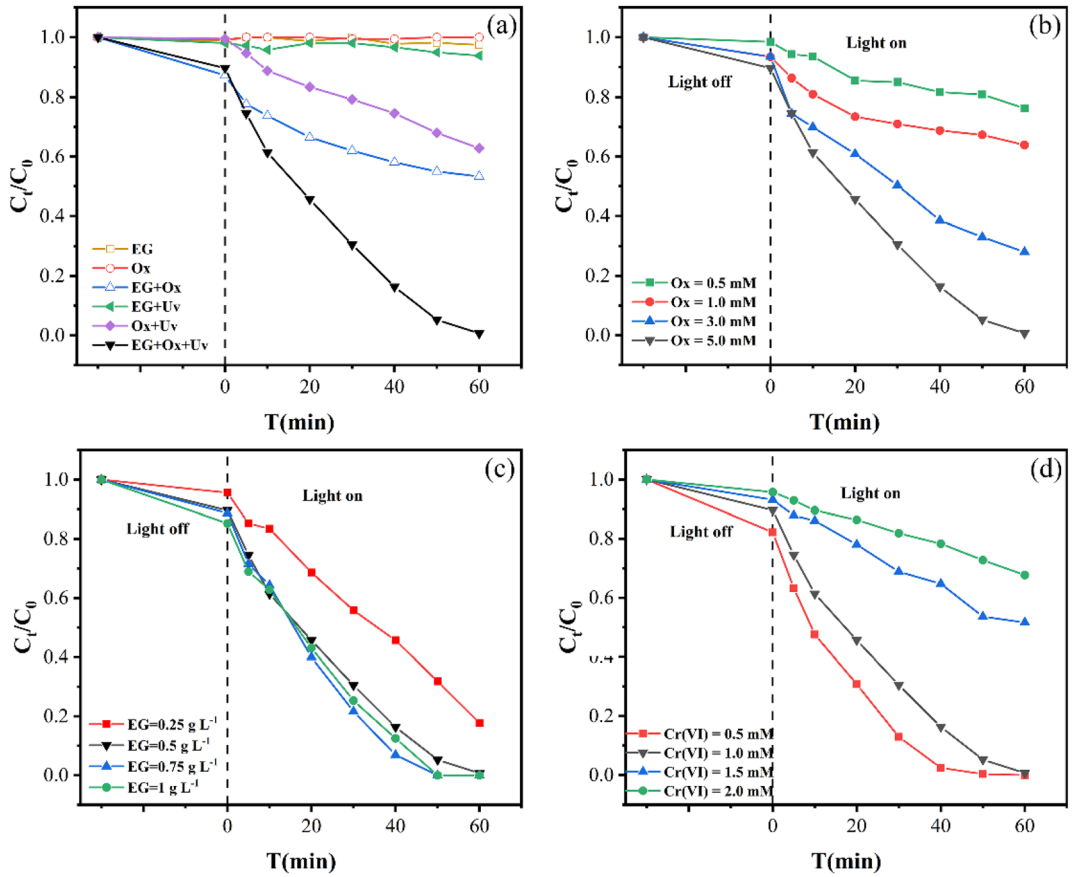

Fig. 1 (a) The elimination of Cr(VI) in various systems, (b) the impact of the initial Ox concentration in EG + Ox + UV system, (c) the impact of the EG dosage in EG + Ox + UV system, (d) the impact of the initial Cr(VI) concentration in EG + Ox + UV system.

extent, which may be caused by a specific electron transfer between EG, Ox, and Cr(VI). However, the effectiveness of eliminating Cr(VI) still needed to be enhanced.

Under UV irradiation, 37.19% of Cr(VI) was removed by Ox, which was mainly attributed to the Cr(VI) photoreduction through $\cdot CO_2^-$ generated from the photolysis of Ox.[23] The EG + UV system showed a small improvement in Cr(VI) removal (6.19%) compared with EG, indicating the weak light response of EG. Compared to other systems, the EG + Ox + UV system eliminated 99.32% of the solution's Cr(VI) content. This suggested that the addition of EG could efficiently and synergistically improve Ox's ability to remove Cr(VI). Compared with the Cr(VI) elimination performance of the reported graphite-based material and Ox-involved system (Table S1†), the EG + Ox + UV system exhibited an excellent comprehensive elimination efficiency.

A series of thorough analyses of the initial concentration of Ox and Cr(VI), EG dose, co-existing ions, and the reusability of EG in the system were carried out with the goal of eliminating Cr(VI) in the EG + Ox + UV system. The reduction products of Cr(VI) were also confirmed.

3.1.1. Impact of initial Ox concentration in EG + Ox + UV system. In Fig. 1(b), The impact of the initial Ox concentration in the EG + Ox + UV system is depicted. At an initial Ox concentration of 0.5 mM, only 23.79% of the Cr(VI) could be removed. The elimination of Cr(VI) gradually improved to 36.12% and 71.98%, respectively, at the starting Ox concentrations of 1.0 and 3.0 mM. The amount of Cr(VI) in the system was reduced by 99.32% when the initial Ox concentration was introduced at 5.0 mM. The improved elimination of Cr(VI) was directly induced by the higher initial Ox concentration in the EG + Ox + UV system, which might be caused by the higher Ox concentration's ability to produce more reducing species.

3.1.2. Impact of EG dosage in EG + Ox + UV system. Fig. 1(c) shows the impact of the EG dosage in the EG + Ox + UV system. At 60 min, 82.28% of Cr(VI) was removed when the EG dosage was 0.25 g L^{-1}. The elimination of Cr(VI) increased quickly to 99.32% when the EG dosage was raised to 0.5 g L^{-1}. As the EG dosage was raised to 0.75 g L^{-1}, the elimination of Cr(VI) showed a small upward trend (100% of the Cr(VI) in the solution could be eliminated in 50 min). However, when the amount of EG was increased to 1 g L^{-1}, the elimination of Cr(VI) displayed a slight falling trend.

The process of removing Cr(VI) from the EG + Ox + UV system was evaluated for the reaction kinetics by fitting the pseudo-zero-order, pseudo-first-order, and pseudo-second-order rate equations. The obtained rate constant (k) and correlation coefficient (R^2) are displayed in Table 1.

The EG + Ox + UV system's Cr(VI) elimination was most consistent with the pseudo-zero-order kinetic model, according to the highest R^2 value. From Table 1 and the pseudo-zero-order

Table 1 The rate constant (k) and correlation coefficient (R^2) of pseudo-zero-order, pseudo-first-order, and pseudo-second-order kinetics in the EG + Ox + UV system

	Pseudo-zero-order		Pseudo-first-order		Pseudo-second-order	
Dosage of EG	k (mol L^{-1} min^{-1})	R^2	k (min^{-1})	R^2	k (L mol^{-1} min^{-1})	R^2
0.25 g L^{-1}	6.78×10^{-1}	0.998	2.53×10^{-2}	0.944	1.14×10^{-3}	0.79
0.5 g L^{-1}	7.95×10^{-1}	0.965	6.98×10^{-2}	0.883	2.88×10^{-2}	0.471
0.75 g L^{-1}	8.54×10^{-1}	0.941	5.97×10^{-2}	0.948	5.09×10^{-3}	0.745
1 g L^{-1}	7.96×10^{-1}	0.964	4.61×10^{-2}	0.976	2.85×10^{-3}	0.850

kinetic fitting curves in Fig. 2, the rate constant k increased from 6.78 mol L^{-1} min^{-1} to 7.95 mol L^{-1} min^{-1} to 8.54 mol L^{-1} min^{-1} as the EG dosage was raised from 0.25 g L^{-1} to 0.5 g L^{-1} to 0.75 g L^{-1}, respectively. However, the rate constant was reduced to 7.96 mol L^{-1} min^{-1} when the EG dosage was raised to 1 g L^{-1}, which was consistent with the experimental findings. This suggested that a specific EG dosage was crucial for the EG + Ox + UV system to remove Cr(VI). A moderate increase in the EG dose would aid in the elimination of Cr(VI) by increasing the reaction site, whereas an excessive amount of EG would decrease the removal of Cr(VI) by occluding the irradiation of part UV light.

3.1.3. Impact of initial Cr(VI) concentration in EG + Ox + UV system. Fig. 1(d) depicts the impact of initial Cr(VI) concentration in the EG + Ox + UV system. With an initial Cr(VI) concentration of 0.5 mM, the EG + Ox + UV system could remove 99.60% of Cr(VI) in 50 min. At 50 and 60 min, the removal efficiency of 94.77% and 99.32%, respectively, could be achieved when the original Cr(VI) concentration was increased to 1.0 mM. The elimination of Cr(VI) decreased to 48.48% and 32.29%, respectively, at 60 min from the initial Cr(VI) concentrations of 1.5 mM and 2.0 mM, respectively. The reducing species were slowly consumed as the starting Cr(VI) content rose, and the Cr(VI) removal became increasingly inadequate.

3.1.4. Impact of co-existing ions in EG + Ox + UV system. The effect of co-existing ions (1 mM of Cl^-, CO_3^{2-}, NO_3^-, and $H_2PO_4^-$) in the EG + Ox + UV system is shown in Fig. 3(a) to help comprehend the removal of Cr(VI) by the EG + Ox + UV system. At 60 min, the elimination of Cr(VI) by the EG + Ox + UV system was affected differently by the addition of various co-existing ions. No interference was caused by the addition of Cl^- when the EG + Ox + UV system was eliminating Cr(VI). With the addition of NO_3^-, a little increase in the removal of Cr(VI) was observed, which was likely brought on by the radicals that NO_3^- formed when exposed to UV.[24] The elimination of Cr(VI) was weakened by the addition of CO_3^{2-} and $H_2PO_4^-$, which might have been caused by the competing H^+ consumption.

Additionally, how coexisting ions affected the EG + Ox + UV system at 5 min was different from that at 60 min: at 5 min, the Cr(VI) removal was boosted by the inclusion of the four co-existing ions. These might be explained by the short-term increase in conductivity of the solution brought about by the addition of co-existing ions, which favoured the elimination of Cr(VI). The little rise in Cr(VI) elimination with CO_3^{2-} addition over the other three ions might be due to the substantial competitiveness of CO_3^{2-}, for H^+ consumption in the solution.

3.1.5. The capacity to reuse EG in EG + Ox + UV system. In Fig. 3(b), The reusability of the elimination of Cr(VI) by EG in the EG + Ox + UV system is demonstrated. Cr(VI) removal effectiveness decreased from 99.32% in Cycle 1 to 79.86% in Cycle 2, and it continued to fall to 59.39% in Cycle 3 and only 29.32% in Cycle 4. The EG + Ox + UV system's ability to remove Cr(VI) significantly decreased after four cycles of EG use. This might be the result of EG's consumption during the EG + Ox + UV system's elimination of Cr(VI), which also suggested that EG was involved in Ox's photoreduction removal of Cr(VI).

3.1.6. Confirmation of Cr(VI) reduction products. As shown in the inserted illustration in Fig. 3(c) and (d), Cr(VI) was gradually removed from the solution during which the solution's color gradually changed from pale yellow at the beginning to colorless at the end of the Cr(VI) elimination procedure *via* the EG + Ox + UV system. The usage of a UV-vis spectrophotometer was to keep track of the solution throughout the reaction in order to confirm the Cr(VI) reduction products by the EG + Ox + UV system. In the UV-vis spectrum shown in Fig. 3(c), the characteristic peak of Cr(VI) at 350 nm steadily diminished until it vanished. In the meantime, the characteristic peak at 570 nm classified as Cr(III)–Ox complexes[25] gradually emerged and grew over time, as shown in Fig. 3(d). These demonstrated that Cr(VI) had undergone a full reduction and was present as Cr(III)–Ox with Ox.[26]

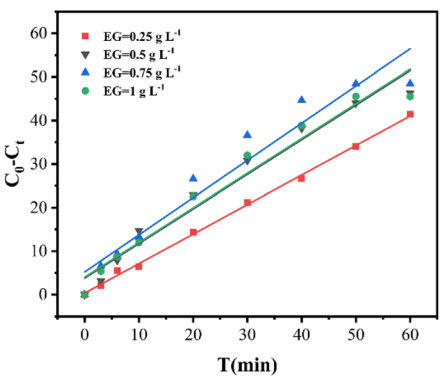

Fig. 2 The pseudo-zero-order kinetic fitting curves for Cr(VI) elimination with different EG dosage.

3.2. Mechanism of Cr(VI) reduction in EG + Ox + UV system

3.2.1. Impact of the EG + Ox + UV system's starting pH. Fig. 4(a) depicts the impact of the starting pH in the EG + Ox +

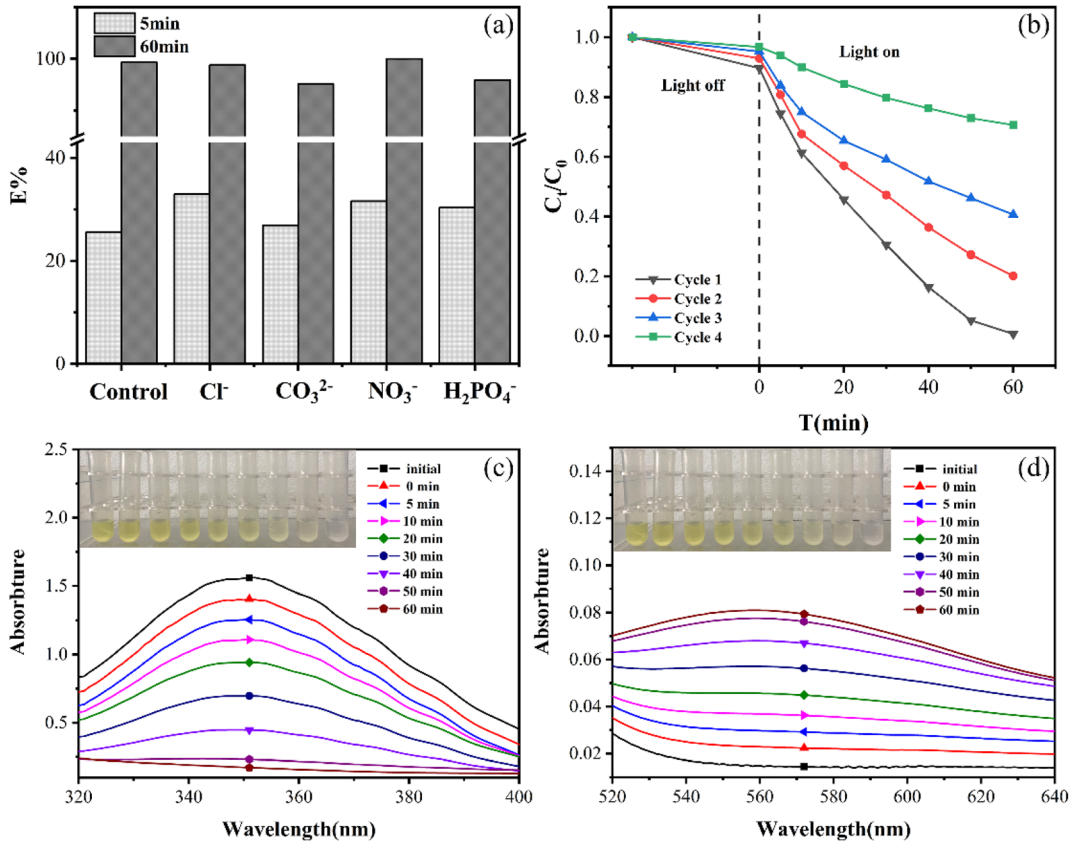

Fig. 3 (a) The impact of co-existing ions in EG + Ox + UV system, (b) the reusability of EG in EG + Ox + UV system, the UV-Vis spectra of the solution at (c) 350 nm and (d) 570 nm during the reaction.

UV system. 99.32% of Cr(VI) had been eliminated at 60 min with a starting pH = 3. The starting pH was raised to 5, and the elimination of Cr(VI) quickly fell to 31.60%. Only 4.49% and 0.76% of Cr(VI) were eliminated from the system when the starting pH values increased to 7 and 9, respectively. It demonstrated that in the EG + Ox + UV system, the acidic environment was more favorable for Cr(VI) photoreduction.

On the one hand, the major existence of Cr(VI) and Ox would vary with the starting pH of the solution, which had different reactivity in the redox reaction. Cr(VI) species were present as $HCrO_4^-$ at pH < 6 or CrO_4^{2-} at pH > 6, respectively. Due to the higher electrode potentials, it was simpler to convert $HCrO_4^-$ to Cr(III) than CrO_4^{2-} ($E_0(HCrO_4^-/Cr^{3+})$ = 1.35 V_{NHE}, $E_0(CrO_4^{2-}/Cr^{3+})$ = 0.56 V_{NHE}).[27] At the same time, the predominated formation of Ox at pH < 4.2 was $HC_2O_4^-$ and $C_2O_4^{2-}$ at pH > 4.2. It could be seen that $HC_2O_4^-$ was more reactive than $C_2O_4^{2-}$ because the power required to rupture the C–C bond in $HC_2O_4^-$ (99.48 kJ mol^{-1}) was substantially lower than that in $C_2O_4^{2-}$ (186.40 kJ mol^{-1}).[27] Because of this, the $HC_2O_4^-$ in the system was simpler to reduce $HCrO_4^-$ at pH = 3 to reach the highest Cr(VI) removal efficiency.

Moreover, $HC_2O_4^-$ (the main existence of Ox at pH = 3) was easily underwent photolysis to $\cdot CO_2^-$ for Cr(VI) photoreduction removal (eqn (2) and (3)).[28]

$$HC_2O_4^- + O_2 + h\nu \rightarrow H^+ + \cdot C_2O_4^- + \cdot O_2^- \quad (2)$$

$$\cdot C_2O_4^- \rightarrow \cdot CO_2^- + CO_2 \quad (3)$$

Additionally, at pH = 3, the oxygen-containing functional groups of EG would be protonated. Then, by electrostatic attraction, part of Cr(VI) and Ox were easily attracted to the surface of EG. After then, a highly active structure among EG, Ox, and Cr(VI) probably formed, which was favorable for electron transport and eventually contributed to lowering Cr(VI).

3.2.2. pH trend variation in the EG + Ox + UV system. In Fig. 4(b), at a starting pH = 3, the Cr(VI) elimination efficiency (E%) and pH variation (ΔpH) ($\Delta pH = pH_t - pH_0$, pH_0 and pH_t are the initial pH and the pH at time t, respectively) at different reaction periods in the EG + Ox + UV system were observed. The trend of the solution's pH increasing steadily along with the increase of E% during the reaction was observed. The solution's pH was 6.7 when Cr(VI) elimination reached 99.32% at 60 min, and ΔpH increased to 3.7. This demonstrated that the H^+ consumption happened in the elimination of Cr(VI) by using the EG + Ox + UV system, which might be primarily due to the Ox consumption in the system.

3.2.3. Trend variation of Ox concentration in EG + Ox system's elimination of Cr(VI). The involvement of Ox in the EG + Ox system was studied as a comparison of the system with UV. The trend variation of Ox concentration in the EG + Ox system's elimination of Cr(VI) is shown in Fig. 4(c). Compared to the weak adsorption removal by EG and almost no reduction by Ox, EG +

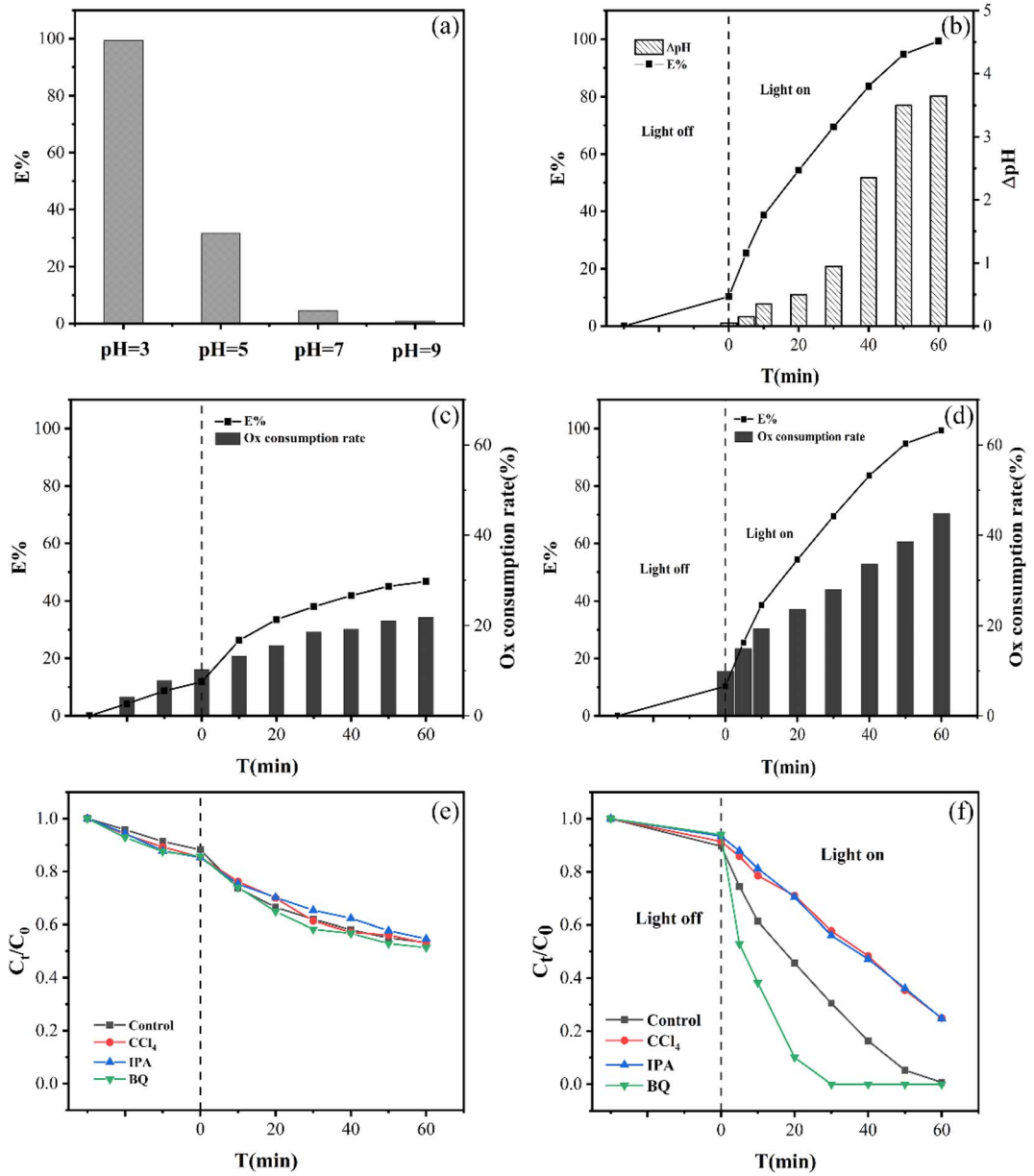

Fig. 4 (a) The impact of the starting pH in the EG + Ox + UV system, (b) pH trend variation in solution of the EG + Ox + UV system, Ox concentration trend variation of (c) the EG + Ox system and (d) the EG + Ox + UV system at pH = 3, effects of free radical scavenging in (e) the EG + Ox system and (f) the EG + Ox + UV system.

Ox exhibited an obvious Cr(VI) removal accompanied by a certain amount of Ox consumption. 21.86% of Ox was consumed by the EG + Ox system to achieve 46.68% elimination of Cr(VI) at 60 min. Ox consumption at this time might be mainly due to the formed highly active structure between EG, Ox, and Cr(VI) (like EG–Ox–Cr(VI)). With the ability to accelerate the direct electron transfer (DET) pathway[15] of EG, the DET pathway in EG–Ox–Cr(VI) might proceed spontaneously, and the progressive conversion from Cr(VI) to Cr(III) would be achieved by the electrons from Ox and EG.

3.2.4. Trend variation of Ox concentration in EG + Ox + UV system's elimination of Cr(VI). The trend variation of Ox concentration during Cr(VI) removal in the EG + Ox + UV system was also monitored, and the results are shown in Fig. 4(d). 9.95% of Ox was consumed and 10.36% of the system's Cr(VI) was eliminated at 0 min of UV exposure. These might be attributed to the DET pathway in EG–Ox–Cr(VI) among Ox, EG, and Cr(VI). From 0 to 60 min of UV exposure, the efficacy of eliminating Cr(VI) soon increased from 10.36% to 99.32%, and the consumption of Ox also increased significantly from 9.95% to 44.79%. In contrast to the EG + Ox system in Fig. 4(c), the EG + Ox + UV system in Fig. 4(d) displayed more notable Cr(VI) elimination and increased Ox consumption. Firstly, UV irradiation would decompose part of Ox to produce $\cdot CO_2^-$ and thus accelerate the Cr(VI) reduction (eqn (4)). Then, upon UV exposure, Cr(VI)–Ox complexes formed by Cr(VI) and Ox would produce a little $\cdot C_2O_4^-$ (ref. 26) and eliminate Cr(VI) with $\cdot CO_2^-$ through the photoinduced electron transfer (PET) pathway (eqn

(3) and (5)). Thirdly, a large part consumption of Ox caused by the significant synergistic effect between EG–Ox–Cr(VI) and UV would generate faster inner electron flow to reduce more Cr(VI) through the higher efficient spontaneous DET pathway in the EG–Ox–Cr(VI).

$$Cr(VI) + \cdot CO_2^- + H^+ \rightarrow Cr(III) + CO_2 + H_2O \quad (4)$$

$$Cr(VI)\text{–}Ox + h\nu \rightarrow Cr(III)\text{–}Ox + \cdot C_2O_4^- \quad (5)$$

3.2.5. Radical scavenging experiments. As shown in Fig. 4(f), the radical scavenging experiments (1 mM CCl_4, IPA, BQ) were used as scavengers for carbon dioxide radicals ($\cdot CO_2^-$), hydroxyl radicals ($\cdot OH$) and superoxide radicals ($\cdot O_2^-$), respectively, to confirm the active substances for Cr(VI) photoreduction in EG + Ox + UV system, and the same experiments were also compared in the EG + Ox system shown in Fig. 3(e).

According to Fig. 4(f), the EG + Ox + UV system's ability to remove Cr(VI) decreased with the addition of CCl_4 from 99.32% to 75.06%, demonstrating the presence of $\cdot CO_2^-$ active species in the Cr(VI) removal process. $\cdot CO_2^-$ played an active species role in Cr(VI) elimination by the system, which was beneficial to Cr(VI) reduction. When $\cdot OH$ was caught by IPA, the elimination of Cr(VI) decreased to 75.20%, demonstrating the presence of $\cdot OH$ in the system. $\cdot OH$, as the products of Ox photolysis (eqn (6)),[29] could oxidize Ox to $\cdot CO_2^-$ and thus improve the system's ability to eliminate Cr(VI) (eqn (7)).[30] The capture of $\cdot OH$ would limit the generation of $\cdot CO_2^-$, which prevented the EG + Ox + UV system from photo-reducing Cr(VI). The Cr(VI) elimination in the system rose greatly (100% at 50 min) when BQ was added to the system to capture $\cdot O_2^-$, demonstrating that $\cdot O_2^-$ impeded the Cr(VI) elimination. The reaction between the oxygen in the air and the $\cdot CO_2^-$ in the EG + Ox + UV system resulted in the generation of $\cdot O_2^-$ (eqn (8)).[31] A part of $\cdot CO_2^-$ would be consumed in the production of $\cdot O_2^-$, and $\cdot O_2^-$ as oxidative radicals would also expand reducing species within the system. When $\cdot O_2^-$ was captured, the amount of reducing species would increase, then the efficiency of Cr(VI) reduction would be improved.

$$Ox + h\nu \rightarrow \cdot OH + \cdot OCCOOH \quad (6)$$

$$Ox + \cdot OH \rightarrow \cdot CO_2^- + H_2O \quad (7)$$

$$\cdot CO_2^- + O_2 + H^+ \rightarrow CO_2 + HO_2/\cdot CO_2^- \quad (8)$$

While in Fig. 4(e), the scavenging of radicals had little impact with regard to the EG + Ox system's elimination of Cr(VI), demonstrating that the system was not affected by free radical action. The EG + Ox system's Cr(VI) elimination might have been largely caused by the spontaneous DET pathway in the formed EG–Ox–Cr(VI).

3.3. The function of EG in EG + Ox + UV system's elimination of Cr(VI)

Data using SEM, XRD, FT-IR, XPS, Mott–Schottky as well as EIS curves of EG and EG after reaction were collected to further explore the function of EG in the EG + Ox + UV system's elimination of Cr(VI).

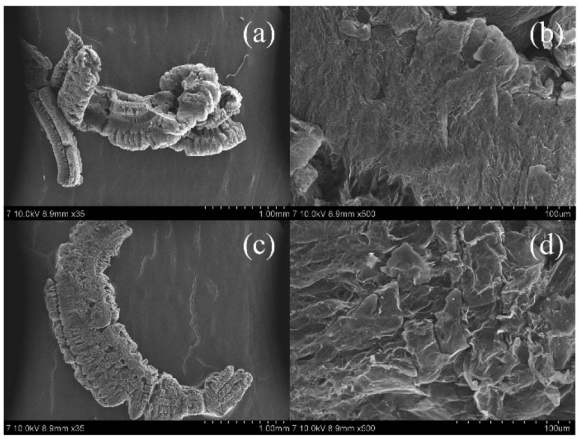

Fig. 5 SEM images of EG (a, b) and EG after reaction (c, d).

Surface morphologies of EG and EG after the reaction were analyzed by SEM. At low magnification, EG after the reaction in Fig. 5(c) maintained the same worm-like structure as well as the

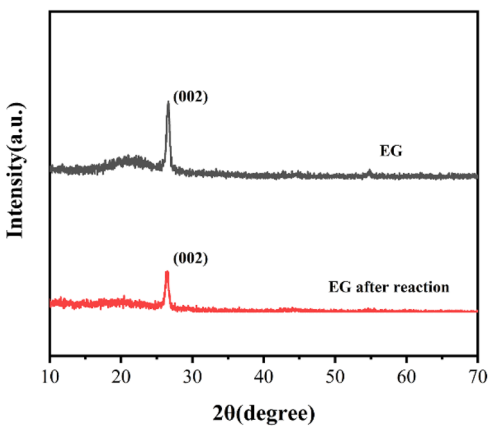

Fig. 6 XRD patterns of EG and EG after the reaction.

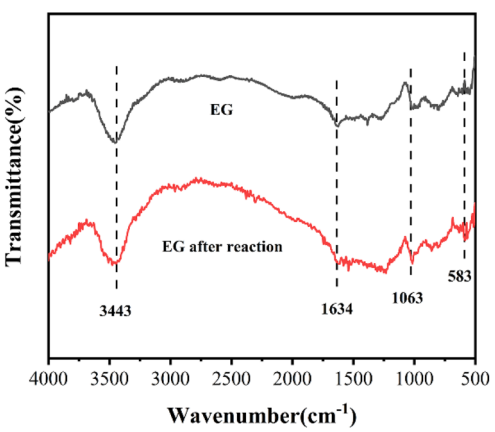

Fig. 7 FT-IR patterns of EG and EG after reaction.

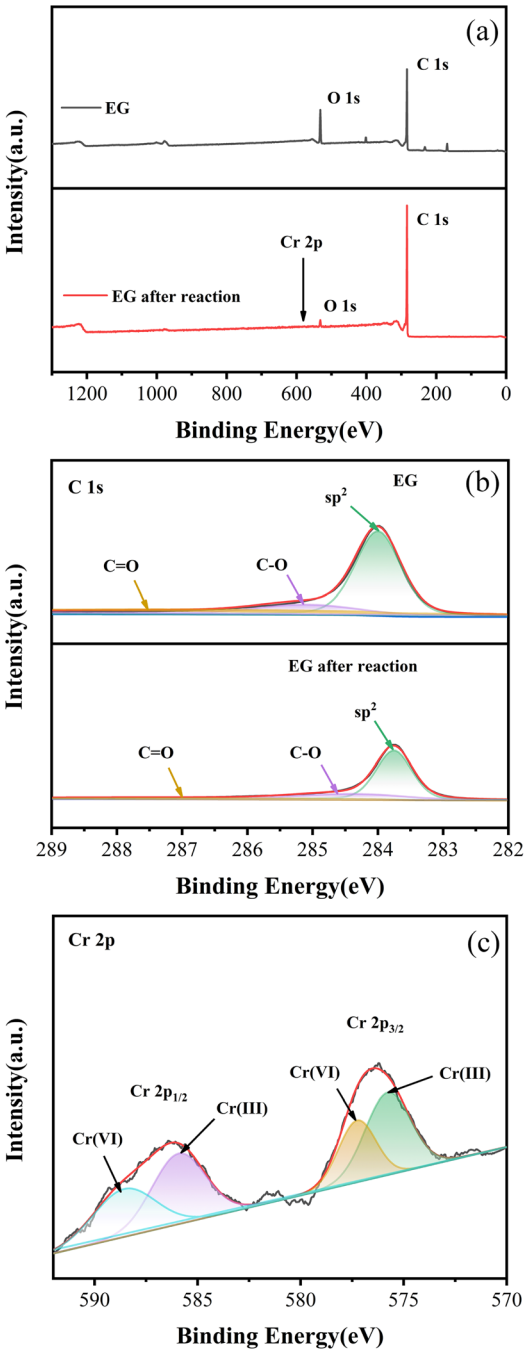

Fig. 8 XPS spectra of EG and EG after reaction: (a) survey, (b) C 1s in EG and EG after reaction, (c) Cr 2p in EG after the reaction.

EG in Fig. 5(a). At higher magnification, the surface appearance of EG after the reaction in Fig. 5(d) was different from that of EG in Fig. 5(b). EG appeared as a flatter layered-graphite structure, while EG after the reaction presented the stripped graphite layer with the bumpy and irregular morphology structure. This might be due to the graphite layers of EG being changed after participating in the process of Cr(VI) elimination.

XRD was also analyzed on EG and EG after the reaction in Fig. 6. Both EG and EG after the reaction showed a characteristic diffraction peak of graphite crystal face (002) at the position of 2θ = 26.48°, corresponding to the formation of curling, overlapping, or stacking of the multilayer graphene structure in EG.[32] While the intensity of the diffraction peak of EG after the reaction decreased compared with EG, which indicated the disorder in the crystal structure inside EG after the reaction.[19] This might be due to the exfoliation of the internal flake graphene structure during the reaction process.

Fig. 7 depicts the FT-IR patterns of EG and EG after the reaction. Compared to EG, the intensity of the peak ascribed to the C–C stretch at 1634 cm^{-1} decreased[33] and that of the peak belonging to C–O at 1063 cm^{-1} increased in the EG after the reaction, which could be explained by the participation of C–C of EG and the formed C–O in Cr(VI) reduction. A new peak at 583 cm^{-1} appeared in EG after the reaction was credited to the Cr–O stretching vibration,[34] which might be due to the creation of EG–Ox–Cr(VI).

XPS survey spectra of EG and EG after the reaction are displayed in Fig. 8(a). The C 1s (binding energy = 284.80 eV) and O 1s (binding energy = 531.08 eV) peaks were dominant in the XPS spectrum of EG and EG after the reaction.[35] Compared with EG, C 1s in EG after the reaction increased from 81.7% to 91.1%, and O 1s decreased from 18.6% to 9.1%, which might be mainly caused by the consumption of EG.

In the C 1s spectra of EG and EG after the reaction (Fig. 8(b)), the peak centered at 284.0 eV could be assigned to a C–C bond with an sp^2 orbital,[36] and peaks located at 285.1 eV and 287.4 eV could be indexed to the characteristics of C–O and C=O.[37] Compared to EG, C–C with sp^2 orbital in EG after reaction

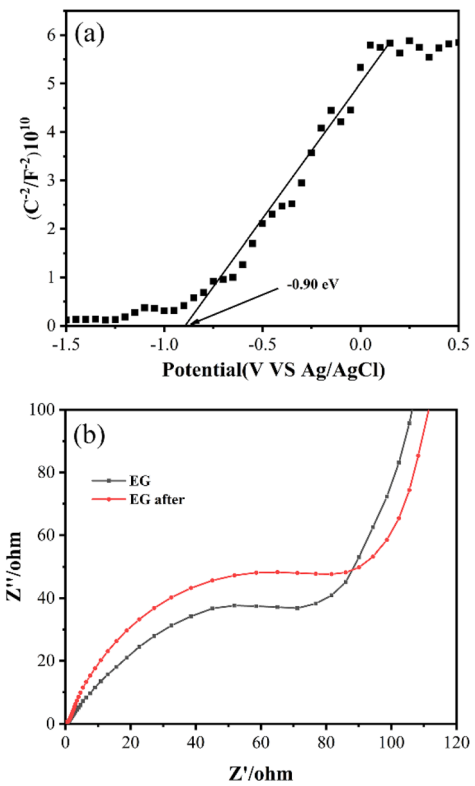

Fig. 9 (a) Mott–Schottky curve of EG, (b) EIS curves of EG and EG after the reaction.

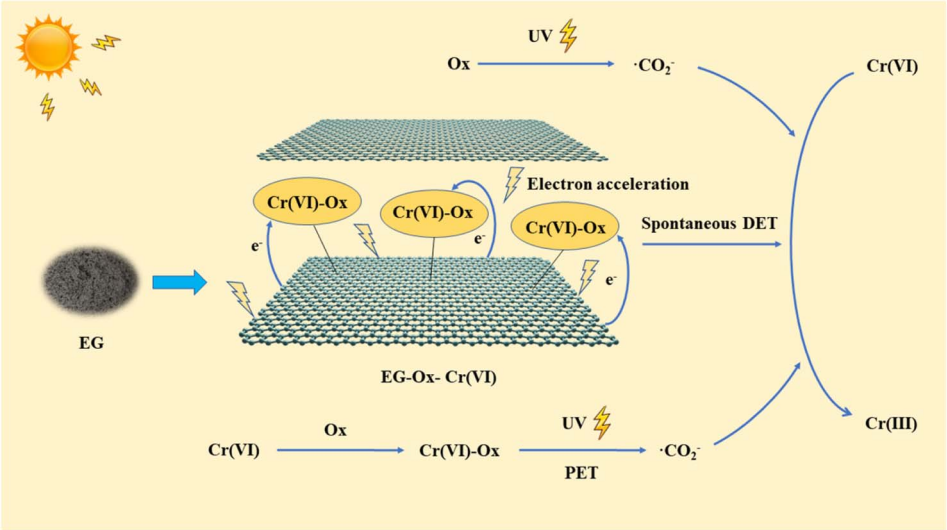

Fig. 10 The possible mechanism for the Cr(VI) elimination in the EG + Ox + UV system.

decreased from 69.9% to 57.5%, while C–O and C=O increased from 12.7% and 17.4% to 21.2% and 21.3%, respectively. This might indicate that C–C with sp^2 orbital was the main group of EG involved in the reaction, which was oxidized to C–O and C=O after donating electrons,[38] which was consistent with the conclusion obtained in the FT-IR spectrum.

Additionally, the survey spectrum of EG after the reaction also showed a minor peak of Cr 2p. In the Cr 2p pattern of EG after the reaction in Fig. 8(c), four peaks at 577.26 eV, 588.56 eV, and 575.77 eV, 585.92 eV could be fitted,[39] indicating strong evidence for the existence of Cr(VI) and Cr(III). Among them, the contents of Cr(VI) and Cr(III) were 40.6% and 59.4%, respectively. The presence of Cr(VI) and Cr(III) species on EG after the reaction might be due to the residue of the formed EG–Ox–Cr(VI) during the EG + Ox + UV system's elimination of Cr(VI).

Mott–Schottky and EIS curves were collected to confirm that EG possessed the ability to give electrons for Cr(VI) reduction. Fig. 9(a) indicated that EG's flat band potential was around −0.90 eV (*vs.* Ag/AgCl, pH = 7), which was comparable to −0.67 V (*vs.* NHE, pH = 7).[40] So the E_{CB} of EG was estimated to be around −0.67 V (*vs.* NHE, pH = 7). A negative value of E_{CB} indicated that EG possessed the potential ability to give its electrons. In the EIS plot, as shown in Fig. 9(b), EG after the reaction had a larger arc radius than EG, implying the higher interfacial charge transfer resistance of EG after the reaction than EG, which resulted in the decrease for EG + Ox + UV system's removal of Cr(VI) after the reuse of EG.

According to the aforementioned investigation, the EG + Ox + UV system's Cr(VI) reduction possible mechanism was mostly made up of three components (Fig. 10): (1) with EG's acceleration effect of the UV exposure, the formed EG–Ox–Cr(VI) with highly active electrons among EG, Ox, and Cr(VI) could effectively achieve the reduction of Cr(VI) within the system through the spontaneous DET pathway; (2) Ox could generate $\cdot CO_2^-$ when exposed to UV to reduce Cr(VI); (3) Cr(VI)-Ox complexes could likewise produce $\cdot CO_2^-$ with UV to eliminate a small portion Cr(VI) by the PET pathway.

4. Conclusions

In this study, we report that the easily-obtained EG with the potential of transferring electrons successfully improved the Cr(VI) photoreduction elimination by environmentally-acceptable Ox. The moderate dosage of EG, the lower pH, and the greater Ox concentration in the EG + Ox + UV system contributed to the removal of Cr(VI). The mechanism of the EG + Ox + UV system's elimination of Cr(VI) was mainly attributed to the synergetic effects of self-reactive reduction (the spontaneous DET pathway in Cr(VI)–Ox–EG with acceleration effect of EG) and photochemical reduction ($\cdot CO_2^-$ produced by photolysis of Ox and the PET pathway in Cr(VI)–Ox complexes). The results of our research provided new ideas for future research on carbon materials in the field of Cr(VI) treatment.

Author contributions

Ling Zhang: conceptualization, resources, writing – review and editing, supervision. Yanqing Sun: investigation, data curation, writing – original draft, writing – review and editing, formal analysis. Jie Sun: investigation, data curation. Fengming Cao: investigation.

Conflicts of interest

There are no conflicts to declare.

Acknowledgements

This research did not receive any specific grant from funding agencies in the public, commercial, or not-for-profit sectors.

Notes and references

1 Y. Zhang, K. Yan, F. Ji and L. Zhang, *Adv. Funct. Mater.*, 2018, **28**, 1806340.
2 P. Johnson, C. Loganathan, V. Krishnan, P. Sakayanathan, V. Raji, S. Vijayan, P. Sathishkumar, K. Murugesan and T. Palvannan, *Environ. Technol.*, 2018, **39**, 1376–1383.
3 L. Du, P. Gao, Y. Liu, T. Minami and C. Yu, *Nanomaterials*, 2020, **10**, 686.
4 F. Cao, Y. Sun, L. Zhang and J. Sun, *Appl. Surf. Sci.*, 2022, **575**, 151583.
5 Y. Liu, S. Xin and B. Jiang, *Environ. Technol.*, 2020, **41**, 430–439.
6 G. Sun, W. Yang and F. Wang, *Int. J. Environ. Res. Public Health*, 2019, **16**, 2771.
7 B. Deng and A. T. Stone, *Environ. Sci. Technol.*, 1996, **30**, 2484–2494.
8 S. Xia, L. Zhang, G. Pan, P. Qian and Z. Ni, *Phys. Chem. Chem. Phys.*, 2015, **17**, 5345–5351.
9 J. Sun, J. D. Mao, H. Gong and Y. Lan, *J. Hazard. Mater.*, 2009, **168**, 1569–1574.
10 W. Niu, J. Sun, L. Zhang and F. Cao, *Chemosphere*, 2021, **262**, 127806.
11 S. M. Lee, I. H. Cho, Y. Y. Chang and J. K. Yang, *J. Environ. Sci. Health, Part A: Toxic/Hazard. Subst. Environ. Eng.*, 2007, **42**, 543–548.
12 Y. Li, C. Chen, Y. Wu, Y. Han and Y. Lan, *Water, Air, Soil Pollut.*, 2017, **228**, 363.
13 C. Gu, M. Cai, P. He, J. Zhu and M. Gan, *Chemosphere*, 2023, **313**, 137557.
14 X. Xu, H. Huang, Y. Zhang, Z. Xu and X. Cao, *Environ. Pollut.*, 2019, **244**, 423–430.
15 D. Kong, Y. Zhao, X. Fan, X. Wang, J. Li, X. Wang, J. Nan and J. Ma, *Environ. Sci. Technol.*, 2022, **56**, 11707–11717.
16 X. Wu, S. Qi, J. He and G. Duan, *J. Mater. Sci.*, 2010, **45**, 483–489.
17 L. Zhang, Y. Wang, S. Jin, Q. Lu and J. Ji, *Environ. Technol.*, 2017, **38**, 2629–2638.
18 H. Jin, J. Yuan, H. Hao, Z. Ji, M. Liu and S. Hou, *Mater. Lett.*, 2013, **110**, 69–72.
19 R. Lan, W. Su and J. Li, *Catalysts*, 2019, **9**, 280.
20 W. Ren, C. Cheng, P. Shao, X. Luo, H. Zhang, S. Wang and X. Duan, *Environ. Sci. Technol.*, 2022, **56**, 78–97.
21 J. Zhang, X. Wang, P. Xia, X. Wang, J. Huang, J. Chen, B. Louangsouphom and J. Zhao, *Res. Chem. Intermed.*, 2016, **42**, 5541–5557.
22 J.-x. Wang, J.-k. Huang and T.-t. Yan, *J. Integr. Agric.*, 2013, **12**, 1267–1278.
23 L. Zhang, F. Cao, J. Sun and Y. Sun, *Environ. Res.*, 2021, **197**, 111070.
24 A. Kumar, A. Rana, G. Sharma, M. Naushad, A. H. Al-Muhtaseb, C. Guo, A. Iglesias-Juez and F. J. Stadler, *ACS Appl. Mater. Interfaces*, 2018, **10**, 40474–40490.
25 N. Chen and B. Pan, *Chem. Eng. J.*, 2020, **387**, 124079.
26 P. Mytych, P. Cieśla and Z. Stasicka, *Appl. Catal., B*, 2005, **59**, 161–170.
27 Y. Mu, X. Jiang, Z. Ai, F. Jia and L. Zhang, *J. Hazard. Mater.*, 2018, **343**, 356–363.
28 D. Jiang, Y. Li, Y. Wu, P. Zhou, Y. Lan and L. Zhou, *Chemosphere*, 2012, **89**, 832–837.
29 G. E. Adams and E. J. Hart, *J. Am. Chem. Soc.*, 1962, **84**, 3994–3999.
30 B. An, H. He, B. Duan, J. Deng and Y. Liu, *Chemosphere*, 2021, **278**, 130388.
31 K. H. Ng, Y.-T. Liu, C. T. Chang, P.-N. Chiang, H. Y. Teah, P. H. Chang and Y.-M. Tzou, *J. Cleaner Prod.*, 2021, **313**, 127726.
32 M. Qiang, H. Xiaomin, L. Ke, D. Rui, H. Zhang, X. Bo and Z. Kewen, *Sep. Purif. Technol.*, 2021, **259**, 118131.
33 W. C. Hung, K. H. Wu, D. Y. Lyu, K. F. Cheng and W. C. Huang, *Mater. Sci. Eng., C*, 2017, **75**, 1019–1025.
34 X. Huang, Q. Hu, L. Gao, Q. Hao, P. Wang and D. Qin, *RSC Adv.*, 2018, **8**, 27623–27630.
35 R. Liu, H. Li, L. Duan, H. Shen, Q. Zhang and X. Zhao, *Appl. Surf. Sci.*, 2018, **462**, 263–269.
36 Y. Du, Z. Tao, J. Guan, Z. Sun, W. Zeng, P. Wen, K. Ni, J. Ye, S. Yang, P. Du and Y. Zhu, *RSC Adv.*, 2015, **5**, 81438–81444.
37 M. Yu, J. Shang and Y. Kuang, *J. Mater. Sci. Technol.*, 2021, **91**, 17–27.
38 Z. Guo, M. Cheng, W. Ren, Z. Wang and M. Zhang, *J. Hazard. Mater.*, 2022, **430**, 128416.
39 H. R. Yang, S. S. Li, C. Yang, Q. D. An, S. R. Zhai and Z. Y. Xiao, *J. Colloid Interface Sci.*, 2022, **607**, 556–567.
40 J. Zheng and Z. Lei, *Appl. Catal., B*, 2018, **237**, 1–8.